DOI: http://doi.org/10.4038/sljp.v23i1.8115

INSTITUTE OF PHYSICS – SRI LANKA

Research Article

Comparison of ZnO nano particles synthesized using sodium hydroxide and triethylamine for photovoltaic applications

G.C. Wickramasinghe[1]*, V.P.S. Perera[1], R. Senthilnithy[2] and C.N. Nupearachchi[1]

[1]*Department of Physics, The Open University of Sri Lanka, Nawala, Sri Lanka*

[2]*Department of Chemistry, The Open University of Sri Lanka, Nawala, Sri Lanka*

Abstract

The formation of zinc oxide (ZnO) nanoparticles were proceeded using the hydrolysis of zinc acetate with sodium hydroxide (NaOH) and triethylamine (TEA). The precipitations from hydrolysis reaction were used to fabricate thin films on Fluorine-doped Tin Oxide glass plates with polyethylene glycol as the binder and triton X-100 as the surfactant by using doctor bade method. Aforementioned ZnO thin films were characterized by X-ray diffraction (XRD) and particle sizes were estimated to be 18 nm and 27 nm in the two samples prepared using NaOH and TEA respectively. Results from UV-Visible spectra and Mott-Schottky measurements were used to calculate the energy band gap to test the suitability of material for photovoltaic applications. The values of photovoltaic efficiencies of fabricated photoanodes of ZnO thin films from NaOH and TEA with N719 dye found to be 0.46 % and 0.79 % respectively.

Keywords: Zinc Oxide (ZnO), Nanoparticles, Sodium Hydroxide, Triethylamine, Photovoltaic

* Corresponding author: gim.chathu@gmail.com

https://orcid.org/0000-0001-5306-5500

1. INTRODUCTION

Metal oxide nanostructures with well controllable size and shape are receiving increasing attention in material synthesis and device fabrication. Zinc oxides is an attractive semiconducting metal oxide due to non-toxicity, low cost and abundance of precursors. Its direct band gap of 3.37 eV and a large exciton binding energy of 60 meV at room temperature has drawn considerable attention of the condensed matter physicists and materials chemists mainly concerning its rich excitonic structure .[1] Due to these unique properties, it has been used to develop and improve the performance of many applications such as ultraviolet (UV) lasers, construction of photovoltaic cells, field-effect transistors, gas sensors, biosensors, photocatalysts, field-emission displays and nanogenerators. Different methods have been used to synthesize ZnO nanoparticles with structural modifications with the use of solvothermal, hydrothermal, microwave irradiation, sol-gel combustion and aqueous chemical growth. [2] In this study, thin film of ZnO nanoparticles were synthesized using aqueous chemical growth method which has been deposited on Fluorine-doped Tin Oxides (FTO) glasses using doctor blade method. The main objectives of this study were to synthesise thin film of ZnO nanoparticles on FTO glasses for photovoltaic applications by precipitation from hydrolysis reaction of Zinc acetate with sodium hydroxide (NaOH) and triethylamine (TEA), usage of those ZnO nanoparticles to fabricate thin films and characterise them for morphological, optical and photovoltaic properties.

2. METHODOLOGY

2.1. Preparation of ZnO thin film

In this study, two samples of ZnO nanoparticles were prepared from 0.1 $moldm^{-3}$ Zinc acetate ($Zn(CH_3COO)_2.2H_2O$) solution with 1 $moldm^{-3}$ of sodium hydroxide (NaOH) and triethylamine (TEA) separately. Zinc acetate (99.5%) was dissolved in distilled water to prepare 0.1 $moldm^{-3}$ zinc acetate solution. The precipitate of zinc hydroxide ($Zn(OH)_2$) of the two samples were synthesized using 10 ml of zinc acetate mixing with NaOH and TEA at room temperature. The pH of the solutions were set at 6 by varying the amount of 1 $moldm^{-3}$ of NaOH and triethylamine (TEA) added to obtain precipitation of zinc hydroxide. The precipitate of each samples were washed three times with deionized water using centrifugation at 3600 rpm for 1 minute to remove excess NaOH and TEA in the precipitate. Finally, they were dried at 100 °C in an oven for 15 minutes.

The each fine paste of both samples were obtained by adding 1 ml of methanol, 2 drops of polyethylene glycol (PEG) and 2 drops of triton X-100 into 25 mg of the ZnO sample. The mixture of the sample was ground in the mortar using a pestle for 15 min to obtain fine paste. The ZnO thin films were prepared on FTO glasses .FTO glass plates were cut into the size of 1 cm × 2 cm which were cleaned in an ultrasonic bath using 1 drop of conc. HNO_3 in distilled water and again with distilled water for 5 minutes. Washed glass plates were boiled in isopropyl alcohol (99.9%) at 80 ˚C for 15 minutes on a hot plate. The two drops of the paste of the each sample was spread on the conducting side of the FTO glass sheets by using doctor blade technique and dried using a hair dryer to obtain thin films. The area of the films were 1 cm^2. Then the films coated plates were sintered in a furnace at 550 ˚C for 2 hours. The ZnO powder samples from sintered thin films were collected for X-Ray Diffraction (XRD) measurements and UV-visible spectroscopic analysis.

2.2. Preparation of photovoltaic cell

Sintered ZnO Films were coated with Ruthenium (N719) dye. Two samples of ZnO films were soaked separately in 2 ml of dye for 24 hours. After that, the dye coated ZnO thin films were washed with alcohol to remove excess dye molecules on surface of ZnO nanoparticles and dried using a hair dryer. The two samples of ZnO films from sodium hydroxide and triethylamine were labeled as ZnO-NaOH and ZnO-TEA respectively.

In this work, the photovoltaic cells were assembled with the counter electrode and ZnO photoanodes of each sample. The conducting side of the counter electrode (platinum sputtered conducting tin oxide glass) and dye absorbed ZnO film used as working electrode were sandwiched and held with clamps. The capillary space in between the two electrodes were filled with electrolyte which was prepared by using 0.83 g of potassium iodide (KI) and 0.127 g of iodine (I_2) that were added into a solution containing acetonitrile and ethylene carbonate at 8:2 ratio.

2.3. Characterization of ZnO nanoparticles and ZnO thin films

The structural properties of the ZnO particles of samples were investigated using high energy X-Ray Diffraction (XRD) analysis. XRD pattern was obtained using a Rigaku Ultima IV. Cu Kβ radiation with a scanning angle (2θ) ranges from 20 ° to 80°. The films of ZnO were characterized by the Mott-Schottky (MS) measurements using a computer coupled with Metrohm Autolab PGSTAT204 to find the flat band potential. The MS performances of the

prepared ZnO thin films were evaluated using a three-electrode configuration with ZnO thin film on FTO, Ag/AgCl electrode and Pt Electrode as working electrode, reference electrode, and counter electrode respectively. The electrolyte used was 10 mM sodium acetate (CH_3COONa) solution at pH 6.5.The optical energy band gap of ZnO nanoparticles were characterized using the UV-Visible spectrophotometer (Genesys 10s UV-Vis). Photovoltaic characteristics of the photovoltaic cells of both samples were measured by using computer coupled with PV power analyzer (VK-PA-100) under illumination of 100 $mWcm^{-2}$ light. Fourier transform infrared (FTIR) spectra of photoanodes were taken in the range of 4000-500 cm^{-1}. The spectra were taken by FTIR-ATR method.

3. RESULTS AND DISCUSSION

The precipitation formation from aqueous zinc acetate ($Zn(CH_3COO)_2.2H_2O$) solution with 1 M of sodium hydroxide (NaOH) and triethylamine (TEA)) can be described according to the equations (1) to (5).

$$Zn\,(CH3COO)_2\,.\,2H_2\,O\,_{(aq)} \rightarrow CH_3COO^-{}_{(aq)} + Zn^{2+}{}_{(aq)} + 2H_2O_{(l)} \quad (1)$$

$$NaOH_{(aq)} \rightarrow Na^+{}_{(aq)} + OH^-{}_{(aq)} \quad (2)$$

$$[TEA]_{(l)} + H_2\,O_{(l)} \rightarrow [TEA]^+{}_{(aq)} + OH^-{}_{(aq)} \quad (3)$$

$$Zn^{2+}{}_{(aq)} + 2OH^-{}_{(aq)} \rightarrow Zn(OH)_{2\,(s)} \quad (4)$$

$$Zn\,(OH)_{2(s)} + 2H_2O_{(l)} \rightarrow Zn(OH)_4{}^{2-}{}_{(s)} + 2H^+{}_{(aq)} \quad (5)$$

$$Zn\,(OH)_4{}^{2-}{}_{(s)} \rightarrow ZnO_{(s)} + H_2O_{(l)} \quad (6)$$

Chemical reactions in equations (1), (2), (4) and (6) are responsible to form precipitate when NaOH is added to the aqueous $Zn(CH3COO)_2\,.2H_2O$ solution. TEA cause hydrolysis and generate OH^- ions, as per equation (3). Chemical reactions in equations (3) to (6) are responsible to form precipitate when TEA is added to the aqueous $Zn(CH3COO)_2$ solution. ZnO nanoparticles on FTO were formed in presence of PEG and Triton-x-100 with $Zn(OH)_2$ at 550 ˚C as indicated in equation (6).

3.1. XRD analysis

The XRD measurements were conducted to study the crystalline structure of ZnO in which the intensity of the diffracted data was recorded over 2θ range of 20 °- 80°. X-ray diffraction

patterns of two ZnO samples in Figure 1 confirmed that the particles of ZnO were highly crystalline consistent with Joint committee on Powder Diffraction Standards (JCPDS) card file no 01-070-8072. No characteristics peaks of impurities such as $Zn(OH)_2$ were detected, suggesting that the products obtained were highly pure. The broadening in the X-ray diffraction pattern indicates the nano-crystalline nature of synthesized ZnO. Furthermore, it can be seen that the intensity of the diffraction peaks are higher, implying perfect crystallinity of ZnO. The diffraction peaks at 2θ values of 31.75°, 34.40°, 36.23°, 47.49°, 56.53°, 62.83°, 66.35°, 67.89°, 69.01°, 72.5° and 77.01° corresponds to reflections from different crystal planes of 100, 002, 101, 102, 110, 103, 200, 112, 201, 004 and 202 for ZnO samples respectively. The crystallite size was calculated by using the Debye-Scherrer's equation (7), where λ is the X-ray wavelength, β is the line broadening at the half width of maximum intensity in radians, and θ is the Bragg angle. From the calculations, the average crystallite sizes of ZnO nanoparticles formed by using NaOH and TEA found to be around 19 nm and 28 nm respectively.

$$D=0.9\lambda/\beta\cos\theta \qquad (7)$$

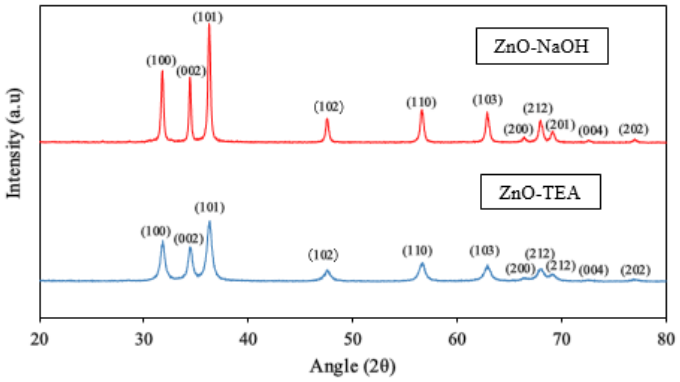

Figure 1: XRD spectrum for two samples of ZnO

3.2. UV-visible analysis

The UV-visible spectra for samples of ZnO nanoparticles synthesized using zinc acetate with NaOH and TEA at pH 6 are shown in Figure 2. As can be seen from this figure, the common peak of maximum absorption for two samples exhibit approximately around 379 nm. This strong peak is attributed to the band gap excitation of zinc oxide. [3] The band gap energy (E_g) of zinc oxide samples is calculated by substituting the value of the wavelength at absorption peak following equation (8).[3], where Plank constant is 4.14×10^{-15} eVs, velocity

of light is 2.99 x 10^8 ms^{-1} and λ_g is the wavelength at peak point and the results are summarized in Table 1.

$$E_g = h\upsilon_g = hc/\lambda_g \quad (8)$$

Table 1. Determination of band gap energy from UV - visible absorption spectra

Sample code	ZnO-NaOH	ZnO-TEA
Wavelength (nm)	381 ± 1	373 ± 1
Band gap energy (eV)	3.26 ±0.01	3.32 ± 0.01

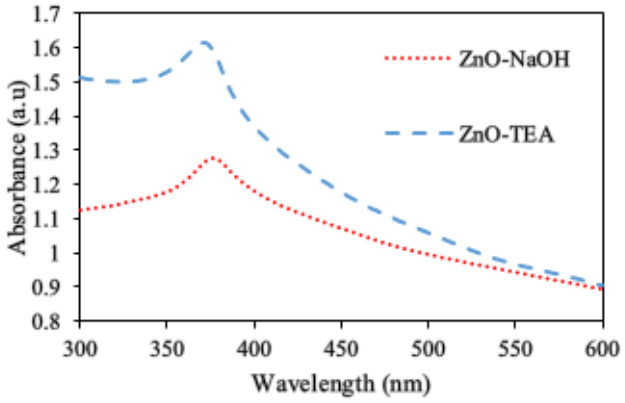

Figure 2: UV-visible absorption spectrum for two samples of ZnO nanoparticles

3.3. Mott-Schottky (MS) analysis

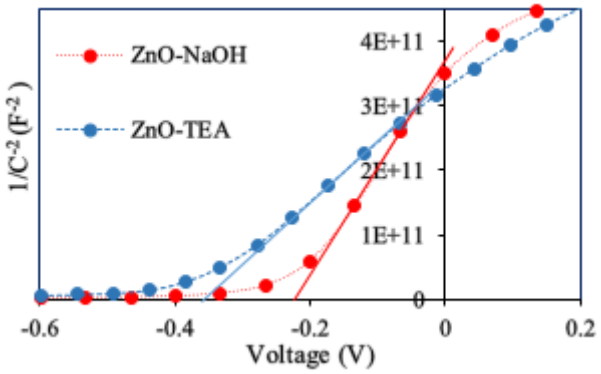

Figure 3: Mott-Schottky plot for thin films of two samples of ZnO

The MS measurement was carried out on the two samples of ZnO thin films on FTO glass as shown in Figure 3. The flat band potential of each sample of ZnO nanoparticles has been obtained from the intercept of the graph plotted potential vs reciprocal square capacitance.

The flat band potentials of two samples of ZnO thin films (E_{FB}) from NaOH and TEA were determined as -0.22 and -0.36 V vs. Ag/AgCl, respectively in a 0.01 moldm^{-3} sodium acetate solution of pH 6.5. Generally, the potential measured against an Ag/AgCl reference can be converted into Normal Hydrogen Electrode (NHE) potential by using equation (9).

$$E_{FB\ (vs\ NHE)} = E_{FB\ (\ pH\ vs\ Agcl\ )} + E_{Agcl} + 0.059 \times pH \qquad (9)$$

The measured pH value of the electrolyte is approximately 6.5, and E_{AgCl} = 0.197 V. Therefore, the calculated flat-band positions of ZnO are 0.02 and -0.13 vs. NHE (pH 0). With band gap energy and conduction band positions of two samples, the valance band of synthesized ZnO samples with NaOH and TEA are estimated to be 3.24 and 3.19 vs. NHE (pH 0) respectively.

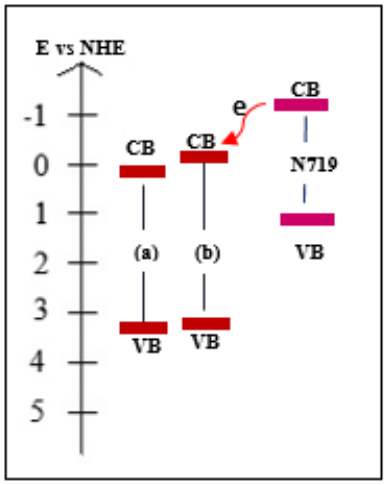

Figure 4: The schematic diagram of the energy band edge positions of (a) ZnO-NaOH, (b) ZnO-TEA and Ruthenium (N719) dye.

3.4. Photovoltaic characterization

Figure 5 (a) illustrate the dark IV curves for the photoanodes of ZnO. The photoanode made by using TEA was given better diode characteristic curve. Figure 5 (b) shows the short circuit current density (J_{sc}) and open circuit voltage (V_{oc}) characteristics of photovoltaic cell fabricated with ZnO photoanodes using the ruthenium (N719) dye under illumination of 100 mWcm^{-2} light source. Solar cell parameters extracted from the J-V curves are tabulated in Table 2. It can be observed that the photoanode of synthesized ZnO nanoparticles with NaOH possessed an efficiency of 0.46 %. In comparison, higher efficiency of 0.79 % were obtained for the photoanodes which were synthesized by using TEA. The increase in J_{sc}, V_{oc}

and fill factor might be involved to improve the light harvesting efficiency of this photoanode.

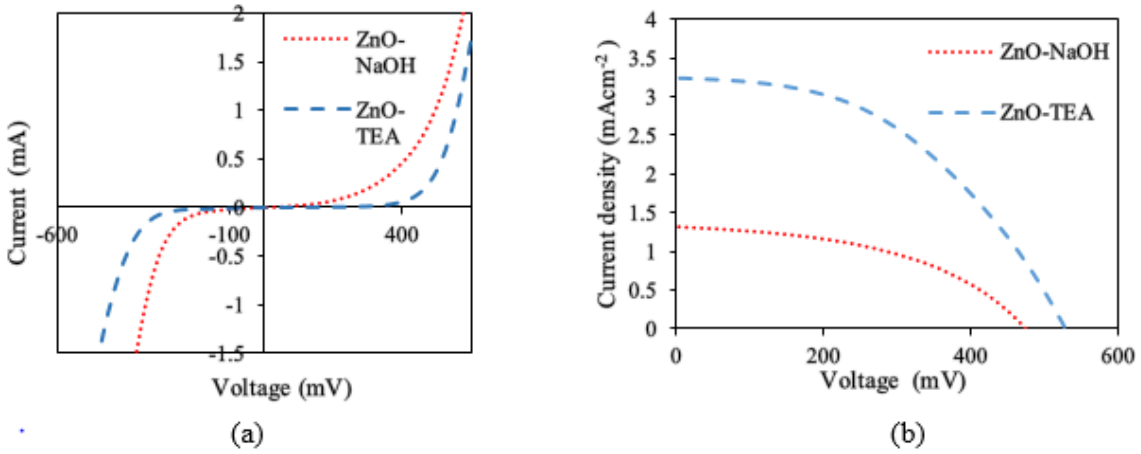

Figure 5: (a) Dark IV curves and (b) J-V characterizations for the two samples of ZnO

Table 2: Photovoltaic measurements, fill factor and efficiency of photovoltaic cell for two samples

Sample	Current density ($mAcm^{-2}$)	Voltage (mV)	Fill Factor (%)	Efficiency (%)
ZnO-NaOH	1.33	476.6	29.3	0.46
ZnO-TEA	3.25	529.6	45.9	0.79

3.5. FTIR analysis of photoanodes

FTIR is an effective method to reveal the dye attachment of composition of synthesized two samples of ZnO. FTIR spectra is evident that ZnO-TEA sample have more N179 dye absorption compare with the absorption peaks presence in FTIR spectra of ZnO-NaOH sample. Figure 6 clearly shows absorption peak around 550 cm^{-1} corresponds to the presences of ZnO in samples. The presence of band at 3378 cm^{-1}, indicates the interaction of Zn with the OH group of ZnO-TEA with N719 dye. Figure 6 shows FTIR spectra functional groups of N719 dye attachment on the two samples of zinc oxide nanoparticles. After the dye-adsorption process, all vibration peaks related to N719 dye molecules (2105, 1609, 1376, and 783 cm^{-1} in Figure 6) were clearly observed in the spectra of ZnO-TEA sample compare with ZnO –NaOH sample. The peak at 2105 cm^{-1} indicates the thiocyanate (NCS) group of the ruthenium-NCS bond which is observed only in spectra of ZnO-TEA [5]. The peak at 1606 cm^{-1} of samples refer to the asymmetric vibration mode of the COO-

group caused by physisorption and chemisorption of N719 dye. The peak at 1378 cm^{-1} indicates the symmetric vibration mode of the COO- group in the chemical bond between N719 and ZnO [5]. The peak at 783 cm^{-1} in spectra of ZnO-TEA refer to =C− H vibrations [6]. The peaks around 880 cm^{-1} presence in spectra of ZnO-TEA corresponds to C− C stretching of residual PEG binder. [7] FTIR spectra provide evidence that ZnO-TEA sample have more N179 dye absorption compare with the absorption peaks presence in FTIR spectra of ZnO-NaOH sample.

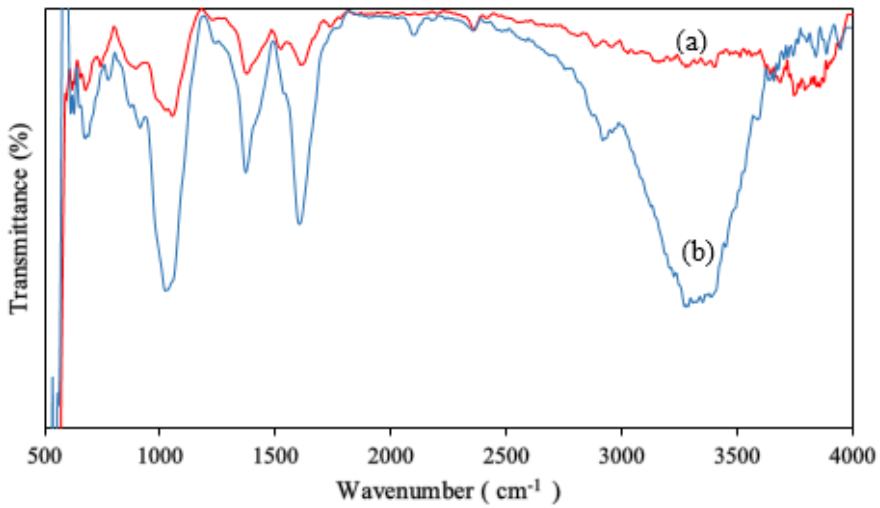

Figure 6: FTIR spectra of N719 dye fabricated ZnO photoanodes (a) ZnO-NaOH and (b) ZnO -TEA

4. CONCLUSION

In Summary, The thin films of two nanoparticle samples of n-type ZnO were successfully synthesized by reaction of aqueous zinc acetate with sodium hydroxide and triethylamine. The thin films of ZnO were developed by using the doctor blade technique on the FTO glasses. According to the XRD results the average particle sizes of ZnO nanoparticles synthesized from NaOH and triethylamine (TEA) are 18 nm and 28 nm respectively. The analysis of UV-visible spectra and Mott-Schottky Measurements revealed the energy band gap for the samples of ZnO and energy band positions for two samples. Under the photovoltaic characterizations, the highest efficiency was recorded for the thin film of ZnO synthesized from aqueous zinc acetate with triethylamine (ZnO-TEA) with 0.79 %.

5. ACKNOWLEDGEMENT

The authors are grateful for the financial support received from the competitive research grant (GRCS201801) of the Open University of Sri Lanka.

6. REFERENCES

1. Zhang, Y., Ram, M.K., Stefanakos, E.K., Goswami, D.Y., (2012). *Synthesis, characterization, and applications of ZnO nanowires.* Journal of Nanomaterials. 2012, pp.1-20. doi:10.1155/2012/624520.

2. Thein, M.T, Pung, S-Y., Aziz, A., Itoh, M., (2015). *The role of ammonia hydroxide in the formation of ZnO hexagonal nanodisks using sol–gel technique and their photocatalytic study*, Journal of Experimental Nanoscience. 10(14), pp. 1068-1081.

3. Salahuddin N. A., El-Kemary, M., Ibrahim, E.M., (2015). *Synthesis and Characterization of ZnO Nanoparticles via Precipitation Method: Effect of Annealing Temperature on Particle Size*, Journal Nanoscience and Nanotechnology, 5, pp. 82-88.

4. Lee, C.-P, Chen, P.-W., Li, C.-T. , Huang, Y.-J. , Li, S.-R., Chang, L.-Y., Chen, P.-Y., Lin, L. - Y., Vittal, R., Sun, S.-S. , Lin, J.-J., Ho, K.-C., (2016). *ZnO double layer film with a novel organic sensitizer as an efficient photoelectrode for dye–sensitized solar cells*, J. Power Sources. 325, pp. 209–219.

5. Hirose, F., Kuribayashi, K., Shikaku, M., Narita, Y., Takahashi, Y., Kimura, Y., Niwano, M., (2009). *Adsorption density control of N719 on TiO2 electrodes for highly efficient dye-sensitized solar cells*, Journal of The Electrochemical Society. 156 (9), pp. 987–990.

6. Pang, Chen, C., Chen, L., Liu, W., Wei, M., (2012). *Flexible dye-sensitized ZnO quantum dots solar cells*, RSC Advances .2, pp. 9565–9570.

7. Wongrerkdee, S., Moungsrijun, S., Pimpang P., Hongsith, K., Choopun, S., (2021). *Linking bridge improvement of ZnO/N719 interfaces via ammonia treatment for efficiency enhancement of dye-sensitized solar cell*, Surfaces and Interfaces.23, pp.100991.

INSTITUTE OF PHYSICS – SRI LANKA

Research Article

Preliminary optimization of low-cost quasi solid-state dye sensitized solar cells with multilayer photoanodes, and graphite-based counter electrodes

H. M. N. Wickramasinghe*, K. Wijayaratne and T. M. W. J. Bandara

Department of Physics and Postgraduate Institute of Science, University of Peradeniya, Peradeniya, Sri Lanka.

Abstract

Investigation and development of platinum free counter-electrodes are highly important in preparing low-cost Dye-Sensitized Solar Cells (DSSCs). In this study, low-cost graphite and TiO_2 composite counter-electrodes are investigated along with photo-electrodes containing dye-photosensitized (N719) TiO_2 multilayers (five, six, and seven layers).

The highest DSSC efficiency is observed for the cells assembled using the counter-electrode that contains 80% of graphite and 20% TiO_2, for all the multilayer photo-electrode series investigated. When comparing different series of multilayer photo-electrodes assembled with this optimized counter-electrode composition, the DSSC efficiency for the six-layer series is greater than the five and seven-layer electrodes.

This best composition of electrodes optimizes the efficiency by fine-tuning between the charge carrier transport properties and catalytic activity of the electrode. The graphite content plays a significant role due to its catalycity. In 3 hours under irradiation, open-circuit voltage got reduced by 8.0%, while the current density and efficiency got improved by 43.2% and 7.0%, respectively, as observed for the cells with the optimum electrode combination. It can be determined that Graphite/TiO_2 80%/20% counter-electrodes with six-layer photoelectrodes optimize the performance of platinum free low-cost DSSCs.

Keywords: Dye-sensitized Solar Cell, Low-Cost Counter-electrode, and Graphite/TiO_2 Composite.

* Corresponding author: narmadawick@gmail.com

1. INTRODUCTION

Most of the dye-sensitized solar cells (DSSCs) currently being developed use platinum as the counter-electrode material, which is an expensive material, despite its superior electro-catalytic activity[1,2]. When searching for a cost-effective alternative to platinum, critical properties are conductivity, durability against iodine corrosion, high catalytic activity, and cell stability. Graphite is an emerging replacement for platinum for DSSC counter-electrodes[3]. Most of the testified studies on carbonaceous counter-electrodes have been developed with liquid electrolytes, with adverse effects on cell stability and longevity. The primary issue with carbonaceous counter-electrodes is the insufficient adhesion to the substrate. Overcoming this, leading to good film formation, is crucial in improving the efficiency of the DSSCs while reducing the cost[4]. This study explores an effective solution for these issues by developing composite counter-electrodes consisting of graphite and TiO_2 nanoparticles, along with optimizing the number of layers on photo-electrodes[5]. First, several series of counter-electrodes were developed by altering the chemical composition. Then their performances were investigated by assembling cells with three different multi-layered TiO_2 working electrodes sensitized with N719 dye[6].

To reduce the well-known instability issues in liquid electrolytes, we used an improved gel polymer electrolyte in the presented study[7]. A previously optimized gel polymer electrolyte comprised of 4-tert-butyl pyridine (4TBP), ethylene carbonate (EC), 1-butyl-3 methylimidazolium iodide (BMII), propylene carbonate (PC), lithium iodide (LiI), tetrahexylammonium iodide (Hex_4NI), and polyethylene oxide (PEO) was utilized in this work[2,5].

2. METHODOLOGY

A series of counter-electrodes were developed by mixing graphite and TiO_2. Table 1 shows relevant weights of TiO_2 nanoparticles (21 nm) and commercial graphite powder. A slurry was obtained by adding 0.1M HNO_3 (2 ml) and was then coated on fluorine-doped tin oxide (FTO) substrate. The films were annealed at 450 °C (30 minutes) to complete the counter-electrode preparation.

Table 1. Weight proportions of TiO_2 and graphite in deferent counter-electrodes.

Electrode	Graphite /wt.%	TiO_2 % /wt.%
A	100	0
B	90	10
C	80	20
D	70	30
E	60	40
F	50	50

To investigate the layering effect of photo-electrodes, 5, 6, and 7 layers of TiO_2 were coated on FTO substrates. In the preparation, a slurry of TiO_2 nanoparticles (∽13 nm) prepared by mixing 0.5 g of TiO_2 with 2 ml of (0.1M) HNO_3 was spin-coated at 2300 rpm for around 2 minutes. After air-drying for ∽5 h, the prepared electrodes were sintered at 450 °C for 30 minutes[8]. The 2nd layer was prepared using the same process, by spin coating at 1000 rpm for about 2 minutes. For the 3rd layer, another TiO_2 dispersion was prepared by grinding 0.5 g of larger TiO_2 nanoparticles (∽21 nm) with 2 ml of 0.1M HNO_3[9]. The resultant dispersion was then spin-coated (1000 rpm, 2 minutes) followed by sintering at 450 °C. Then the subsequent 4th, 5th, 6th, and 7th layers were coated by repeating the same method [8]. The prepared electrodes were immersed in a 0.5 mM N719 dye/ethanol solution for 48 h [9]. Finally, a series of DSSCs were assembled by sandwiching the pre-optimized gel electrolyte between the electrodes[10].

Current-voltage (*I-V*) characteristics of Graphite/TiO_2 electrodes were measured to find sheet resistance values. For this purpose, Graphite/TiO_2 films were deposited on a glass substrate. The X-Ray Diffraction (XRD) and Scanning Electron Microscopic (SEM) images were used for the structural and morphological characterization of Graphite/TiO_2 composite counter-electrodes. In order to study the solar cell performance, the DSSCs were irradiated by the solar simulator (AM1.5, 1000 W m^{-2}) and *I-V* parameters were measured.

3. RESULTS AND DISCUSSION

3.1. Structure and morphology of the counter-electrodes

Scanning Electron Microscopic images (SEM) of the six counter-electrodes are given in Figure 1. According to Figure 1, the film with 100% graphite (Fig. 1-A) yields high reflectance at grain boundaries, and the density of such boundaries is higher. In addition, it

was observed that the film formation is poor for this composition. When the TiO_2 content increases, the density of these reflective domains declines, which may be due to the materialization of expanded graphite during the vigorous stirring.

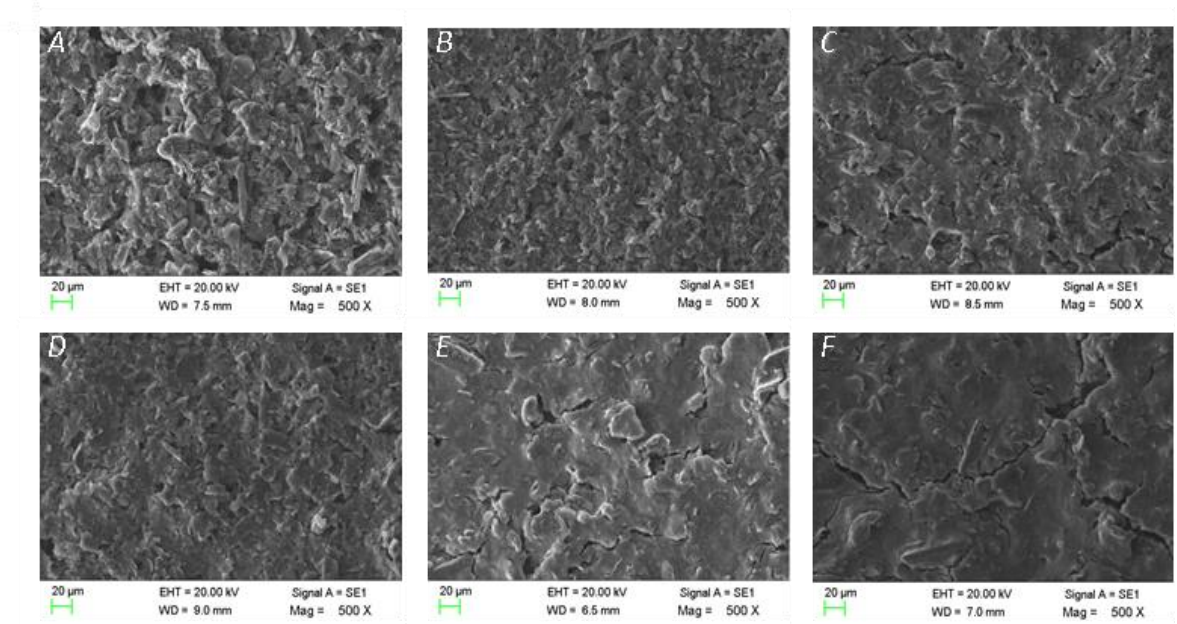

Figure 1: SEM images of counter-electrodes made of Graphite/TiO_2 composite at 500 magnification with varying graphite composition (A) 100% (B) 90% (C) 80% (D) 70% (E) 60% (F) 50% by weight.

The sheet resistance measurements obtained for the Graphite/TiO_2 thin films coated on soda-lime glass plates are given in Table 2. The calculated resistivity and conductivity values are also provided. The average thickness of Graphite/TiO_2 layers was about 0.14 mm. The electrodes with 80% and 70% graphite content demonstrated relatively low sheet resistance and high conductivity. Poor film formation and weak adhesivity to the substrate of 100% graphite samples would have resulted in a slightly lower conductivity. 50% graphite samples demonstrated the lowest conductivity out of all measured samples, which can be attributed to the presence of an excessive amount of low-conducting TiO_2. The highest conductivity value of 1.30 S cm^{-1} was exhibited by the electrode that contained 70 wt.% graphite and 30 wt.% TiO_2.

X-ray diffraction (XRD) was used to investigate the effects of the Graphite/TiO_2 composition on the film structure (Figure 2). XRD spectra in Figure 2 indicate the absence of chemical interactions between TiO_2 and Carbon. However, it can be inferred that the effective exfoliation of graphite into expanded graphite or multilayer graphene has happened since a relative peak broadening is observed with the increasing centration of TiO_2.

Table 2. Resistivity and conductivity values obtained from sheet resistance values of the Graphite/TiO_2 electrodes with various compositions.

Sample	Graphite /wt. %	Sheet Resistance /∧ cm^{-2}	Resistivity /∧ cm	Conductivity /S cm^{-1}
A	100	123.53 ± 0.01	1.73 ± 0.12	0.58 ± 0.04
B	90	89.35 ± 0.01	1.25 ± 0.09	0.80 ± 0.08
C	80	57.56 ± 0.01	0.81 ± 0.06	1.24 ± 0.18
D	70	54.84 ± 0.01	0.77 ± 0.06	1.30 ± 0.20
F	60	63.90 ± 0.01	0.89 ± 0.06	1.12 ± 0.15
F	50	1553.83 ± 0.01	21.75 ± 1.55	0.05 ± 0.00

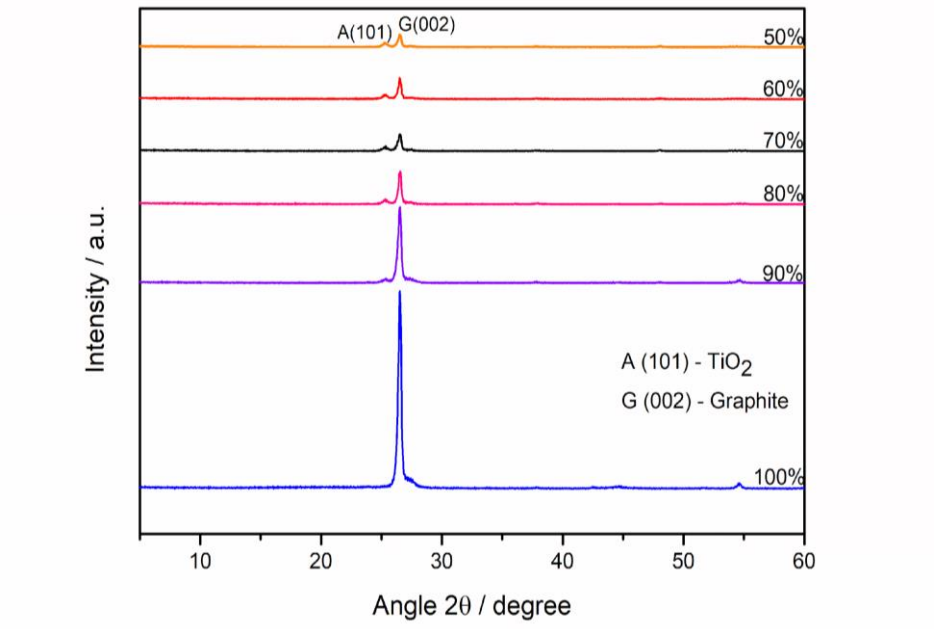

Figure 2: XRD patterns of Graphite/TiO_2 electrode series with different compositions

3.2. Structure and morphology of multilayer photo-anode

XRD spectra of photoelectrodes were used to examine the crystal structure of the photoelectrodes. There were no significant changes among the crystalline structures of 5, 6, and 7 layered TiO_2 films, and thus, the XRD spectrum of six-layered TiO_2 electrodes is shown in Figure 3. All the samples exhibited peaks corresponding to Anatase (101, 004, 200) and Rutile (110, 211, 220, 002, 310) crystal planes.

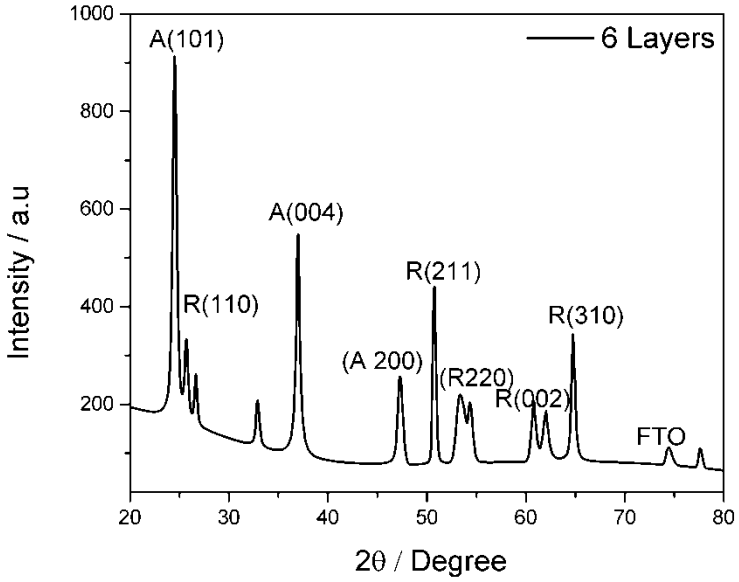

Figure 3: XRD spectra of six-layer photoelectrode

Table 3: XRD analysis data for six-layer TiO_2 film

$2\boldsymbol{\theta}$ / Degree	Peak Height / a.u.	Peak Intensity (a.u.)	FWHM / Degree	*d* Spacing / Å
24.50	746.31	459.39	0.50	3.63
25.70	174.87	135.99	0.46	3.46
37.00	488.38	259.41	0.42	2.43
50.75	359.29	151.75	0.39	1.80
64.75	267.71	159.48	0.45	1.44

3.3 Optimization of counter-electrode composition

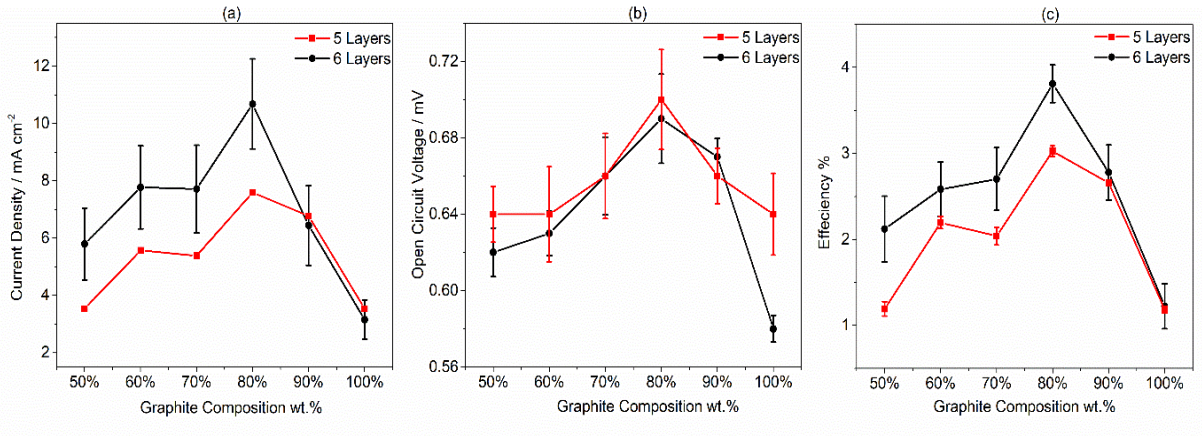

Figure 4. (a) The current density (b) open-circuit voltage and (c) efficiency; versus graphite composition in the counter-electrode for the two series of DSSCs

In order to find the optimum counter-electrode composition, several DSSCs were prepared by changing the composition of the counter-electrode. Two such series were investigated using five and six-layered photo-anodes. Figure 4 shows circuit current density (J_{SC}), open-circuit voltage (V_{OC}), and energy conversion efficiency as a function of graphite composition

in the counter-electrode for both the series of DSSCs. It can be concluded that 80% graphite and 20% TiO_2 containing counter-electrode is optimum for DSSCs. This can be due to the combined effect of the high conductivity of the counter-electrode and the high electro-catalytic activity due to graphite.

3.4 Optimization of the photo-anode

The composition-optimized counter-electrode was selected to study the effect of the number of TiO_2 layers in the photo-anode. The variations of the J_{SC} against the cell potential is shown in Figure 5 (a) in Figures 6 (b), respectively for 5, 6, and 7 -layer series of photoanodes prepared using the above-mentioned optimized counter-electrode.

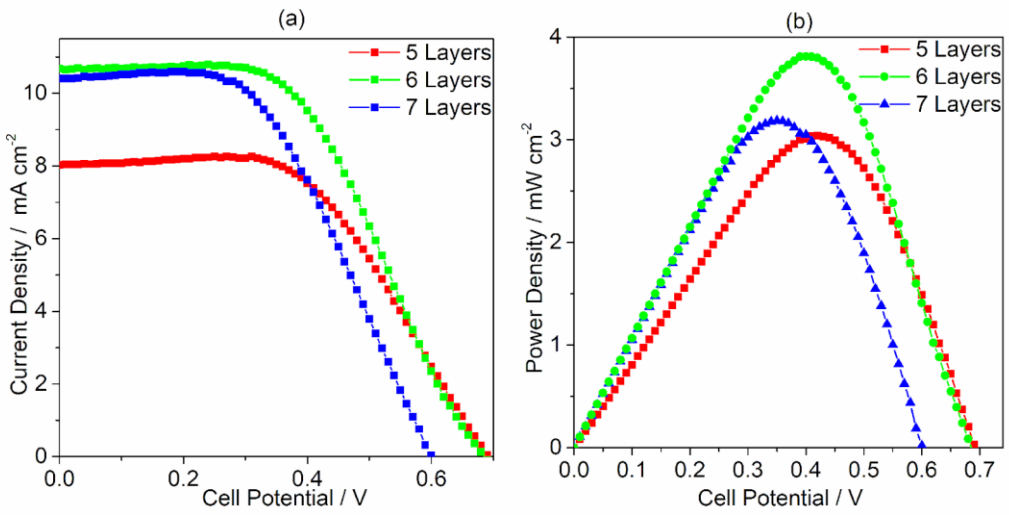

Figure 5. (a) The power density and (b) Current density vs. cell potential for optimized counter electrode (80% graphite)

The highest efficiency (3.81%) was observed for the DSSC with the counter-electrode that contained 80 wt.% graphite with 6-layer photo-anode. This configuration surpassed the efficiency of the counter-electrode with the maximum conductivity (2.7%, at 70 wt.% graphite) due to the greater catalycity of its graphite-rich (80%) composition. J_{SC} and V_{OC} were 10.68 ± 0.345 mA cm^{-2} and 0.69 ± 0.01 mV respectively for DSSCs with six-layer photoanode and optimized counter-electrode. For five-layer photoanode series, the highest efficiency (3.03%) was still exhibited by the DSSC with Graphite/TiO_2 electrode that confined 80 wt.% graphite. The optimized J_{SC} and V_{OC} were 7.59 ± 0.345 mA cm^{-2} and 0.70 ± 0.01 mV.

3.5 Stability

In addition, the short-term stability of the optimized cell was monitored continuously by obtaining *J-V* curves for about 3 hours. Despite the cells being unsealed, they were significantly stable within the three-hour period due to the use of the improved gel polymer electrolyte. The efficiency gradually increased throughout the illumination period and is evident by the dramatic increase in photocurrent density and the drop in V_{OC}. This behavior can mainly be attributed to the ionic conductivity improvement of the electrolyte upon increasing temperature under continuous irradiation. The same phenomena resulted in the drop of the V_{OC} upon increased recombination of excited electrons in the photoelectrode with tri-iodide in the electrolyte. At the end of three hours, V_{OC} was reduced by 8.0%, while J_{SC} improved by 43.2%, leading to an efficiency increase of about 7.0%. It is planned to measure the long-term stability by sealing these quasi-solid state solar cells.

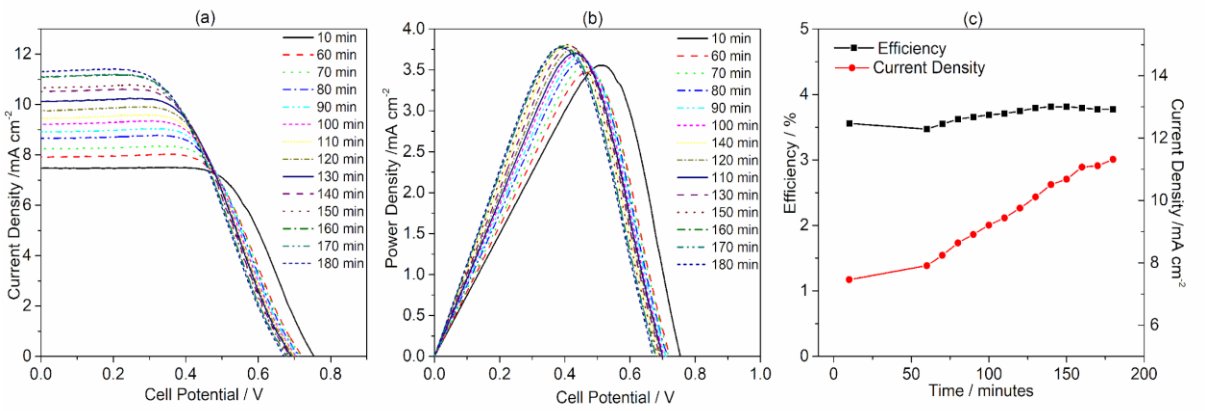

Figure 6. The time dependence of the (a) current density and (b) power density versus cell potential (c) Time verses efficiency and current density variation of DSCs with 80% graphite counter-electrode

4. CONCLUSION

The cost-effective counter-electrodes were developed using TiO_2 nanoparticles and commercial graphite to substitute costly platinum counter-electrodes in dye-sensitized solar cells. The highest DSSC efficiency was observed for the counter-electrode composed of 80% graphite and 20% TiO_2 by optimizing the trade-offs between charge carrier transport and the electro-catalycity. This optimum composition ratio was confirmed by using two series of DSSCs having 5 and 6 TiO_2 layers in the photo-anode.

Further, it was confirmed that the 6 layer TiO_2 photoanode gives the highest DSSC performance by investigating 7 layer photo-anodes alongside 5 and 6 layer versions. The DSSCs gave the highest efficiency (3.81%) with counter-electrodes containing 80 wt.%

graphite with photo-anodes having 6 TiO_2 layers. The optimized cells exhibited very good short-term stability within three hours of continuous illimitation, and there were no traces of efficiency drop. It can be concluded that 6-layer photo-anodes assembled with 80/20 wt.% Graphite/TiO_2 counter-electrode is the optimum electrode combination to prepare cost-effective DSSCs.

Acknowledgment

The authors gratefully acknowledge the support received via the Postgraduate Institute of Science (PGIS), University of Peradeniya research grant (No. PGIS/2020/05).

REFERENCES

[1] Iqbal, M. Z. and Khan, S. (2018) "Progress in the performance of dye sensitized solar cells by incorporating cost effective counter electrodes," *Sol. Energy*, vol. 160, pp. 130–152.

[2] Nishshanke, M., Arof, A. K., and Bandara, T., (2020) "Review on mixed cation effect in gel polymer electrolytes for quasi solid-state dye-sensitized solar cells," *Ionics (Kiel).*, vol. 26.

[3] Salvatierra, R. V., Domingues, S. H., Oliveira, M. M. and Zarbin, A. J. G., (2013) "Tri-layer graphene films produced by mechanochemical exfoliation of graphite," *Carbon N. Y.*, vol. 57, pp. 410–415.

[4] Denaro, T., *et al.*, (2009) "Investigation of low cost carbonaceous materials for application as counter electrode in dye-sensitized solar cells," *J. Appl. Electrochem.*, vol. 39, no. 11, pp. 2173–2179.

[5] Yousif, Q. A., Mahdi, K. M., and Alshamsi, H. A., (2021) "Enhanced photovoltaic performance of dye-sensitized solar cell based on ZnO nanoparticles and ZnO/graphene nanocomposites," *J. Chinese Chem. Soc.*, vol. 68, no. 9, pp. 1637–1643.

[6] Bandara,T. M. W. J., *et al.*,(2015) "Efficiency of 10 % for quasi-solid state dye-sensitized solar cells under low light irradiance," *J. Appl. Electrochem.*, vol. 45, no. 4, pp. 289–298.

[7] Bandara, T. M. W. J., Dissanayake, M. A. K. L., Jayasundara, W. J. M. J. S. R., Albinsson, I., and Mellander, B. E., (2012) "Efficiency enhancement in dye sensitized solar cells using gel polymer electrolytes based on a tetrahexylammonium iodide and MgI 2 binary iodide system," *Phys. Chem. Chem. Phys.*, vol. 14, no. 24, pp. 8620–8627.

[8] Nishshanke,G. B. M. M. M., Thilakarathna B. D. K. K., Albinsson I., Mellander B. E., and Bandara, T. M. W. J.,(2021) "Multi-layers of TiO2 nanoparticles in the photoelectrode and

binary iodides in the gel polymer electrolyte based on poly(ethylene oxide) to improve quasi solid-state dye-sensitized solar cells," *J. Solid State Electrochem.*, vol. 25, no. 2, pp. 707–720.

[9] Bandara, T. M. W. J., Wickramasinghe, H. M. N., Wijayaratne, K., DeSilva, L. A., and Perera, A. A. I., (2020) "Quasi-solid-state dye-sensitized solar cells utilizing TiO2/graphite composite counter electrode and TiO2/N719 sensitizer photoelectrode for low-cost power generation," *J. Mater. Sci. Mater. Electron.*, vol. 32, no. 22, pp. 26758–26769.

[10] Il Kim, M., Cho, J. H., Bai, B. C., and Im, J. S., (2020) "The control of volume expansion and porosity in carbon block by carbon black (CB) addition for increasing thermal conductivity," *Appl. Sci.*, vol. 10, no. 17.